Data-driven LPV Disturbance Rejection Control with IQC-based Stability Guarantees for Rate-bounded Scheduling Parameter Variations

Elias Klauser[1] and Alireza Karimi[2]

***Abstract*— In this paper, the challenge of asymptotically rejecting sinusoidal disturbances with unknown time-varying frequency and bounded rate is explored. A novel data-driven approach for designing linear parameter-varying (LPV) controllers is introduced, leveraging only frequency domain data from a Linear Time Invariant (LTI) Multi-input Multi-output (MIMO) system, eliminating the need for a parametric model. A two-step iterative algorithm is proposed involving convex optimization problems in the frequency domain. Closed-loop stability is ensured using Integral Quadratic Constraints (IQC) that characterize the bounded rate variation of the LPV controller's scheduling parameters. Experimental validation is provided through results obtained on a hybrid micro-vibration damping (MIVIDA) platform tailored for space applications.**

I. Introduction

Disturbance rejection plays a crucial role in control system design, as the presence of noise or external perturbations can significantly impact control performance. Various applications, including active suspension systems [1], optical stabilization [2], control of robotic systems [3], vibration suppression in machinery [4], and active noise-canceling systems [5], [6], heavily rely on effective disturbance rejection strategies. In case the disturbance model is known, control design methods based on the internal model principle (IMP) can be applied. Some non-stationary disturbances can be modeled as a linear parameter-varying (LPV) system with an appropriate scheduling parameter [6] and be integrated into an LPV controller. For practical applications, an upper bound on the variation rate of the scheduling parameter is oftentimes known due to physical limitations of the system.

Model-based control approaches necessitate the availability of an accurate parametric plant model, which typically requires system identification. This system identification step can be time-consuming and consequently expensive, particularly for complex systems. As a result, data-driven control design techniques are gaining prominence in industrial applications, thanks to recent technological developments that provide increased computational power and enhanced sensor technologies. These techniques enable the direct minimization of a control criterion based on measured input-output data, offering a significant advantage in situations where a parametric plant model is either unavailable or challenging to identify.

Frequency response data proves to be effective for the analysis and synthesis of linear control systems, as it can be readily computed from time-domain input-output data, avoiding any modeling errors. The industry widely employs such methods, exemplified by the classic loop shaping technique. Given that most control performance and robust stability conditions can be represented in the frequency domain, recent data-driven methods leverage only frequency-domain data and convex optimization programming to compute LPV controllers [7]–[9]. These methods involve multimodel control optimisation where for a number of selected operating points, a model is generated for frozen scheduling parameters.

The IQC framework, introduced by Megretski and Rantzer [10], offers a versatile mathematical framework for the representation and analysis of various nonlinearities and uncertainties. This includes parametric uncertainties, rate-bounded uncertainties, time-delays, and norm and sector-bounded nonlinearities. The IQC framework enables the establishment of sufficient stability conditions in the frequency domain and allows the analysis of systems with multiple uncertainty types through a single composite IQC.

Data-driven methods combining robust stability and performance analysis within an IQC-based optimization have been explored for designing Multiple-Input Multiple-Output (MIMO) LPV controllers directly from frequency-domain data [8]. This approach has been applied to design LPV controllers for control moment gyroscopes (CMG) in [11]. It is important to note that all presented LPV control design approaches only offer local stability guarantees for frozen scheduling parameters at selected operating points, and stability guarantees for variations in the scheduling parameter are not strictly provided.

In a model-based framework, IQCs have been proposed to guarantee stability for fast and slowly time-varying parameters. Frequency-domain conditions using IQC can be derived to bound the derivative of a time-varying parameter using upper bounds on the structured singular value which can be represented by an LMI in convex optimisation problems [12]. A number of multiplier matrices Π for rate-bounded time-varying real scalars are proposed in the literature [10], [13]. A stability analysis for linear systems with rate-bounded parameters can also be performed using the swapping lemma presented in [14]. The swapping lemma was used to verify the stability of linear systems with slowly varying uncertainties [15]. A similar development was made to analyse linear time-varying parametric rate-bounded uncertainties in [16].

*This work is funded by the European Space Agency ESA Contract No. 4000133258/20/NL/MH/hm.

[1]E. Klauser is with CSEM SA, Rue Jaquet-Droz 1, CH-2002 Neuchâtel, Switzerland, and also with the Laboratoire d'Automatique, École Polytechnique Fédérale de Lausanne, CH-1015 Lausanne, Switzerland elias.klauser@csem.ch

[2]A. Karimi is with the Laboratoire d'Automatique, École Polytechnique Fédérale de Lausanne, CH-1015 Lausanne, Switzerland alireza.karimi@epfl.ch

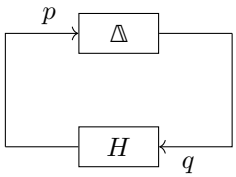

Fig. 1. Basic feedback configuration

In a data-driven framework, A novel LPV controller design approach with stability guarantee for arbitrarily fast variation of scheduling parameters is presented in [17]. The objective of the method is to effectively reject unknown frequency-varying sinusoidal disturbances while ensuring closed-loop stability. The controller is computed from experimental input/output data and no parametric plant model is required. The control system is composed of three main components: an online disturbance frequency estimator using sliding discrete Fourier transform (SDFT), a fixed-structure LPV control part consisting of a time-varying filter, and a stabilising LTI controller. The scheduling parameters of the LPV control part are the harmonic disturbance frequencies estimated with the SDFT algorithm. The method uses the Integral Quadratic Constraint (IQC) framework and convex optimization techniques to design the LPV controller.

This paper is an extension of the work presented in [17] allowing to relax the constraints over stability guarantees for arbitrarily fast time-varying scheduling parameters by including rate bounds in the controller design algorithm. The method is then applied for adaptive disturbance rejection of a hybrid active-passive micro-vibration damping platform (MIVIDA) and achieves much larger variation bounds for the disturbance frequency than the method in [17]. The MIVIDA is a demonstrator for a spaceborne system that was designed to actively isolate a sensitive payload from vibrations present on board of the spacecraft.

The remainder of the paper is organised as follows: First, the notations and the preliminaries are introduced in (Section II). Then, an iterative LPV control design algorithm is presented using constraints on the rate bound of the scheduling parameters to maximize the frequency variation bound in (Section III). The effictiveness of the algorithm is demonstrated by the experimental results in (Section IV). Finally, (Section V) gives some concluding remarks.

II. Preliminaries

Notations: The set of real rational stable transfer functions with bounded infinity norm is denoted by $\mathcal{RH}_\infty$. $A \succ (\succeq)\, B$ indicates that $A - B$ is a positive (semi-) definite matrix and $A \prec (\preceq)\, B$ indicates $A - B$ is negative (semi-) definite. The zero and identity matrices of appropriate size are denoted $\mathbf{0}$ and I respectively. The transpose of a matrix A is denoted by A^T and its conjugate transpose by A^*. Right inverse of A is denoted as $A^R := A^*(AA^*)^{-1}$, and its left inverse is denoted as $A^L := (A^*A)^{-1}A^*$.

A. Integral Quadratic Constraints

In the developments that follow, only discrete-time systems are considered. Two discrete-time signals p and q are said to satisfy the IQC defined by a multiplier Π, if [16]

$$\int_\Omega \begin{bmatrix} P(e^{j\omega}) \\ Q(e^{j\omega}) \end{bmatrix}^* \Pi(e^{j\omega}) \begin{bmatrix} P(e^{j\omega}) \\ Q(e^{j\omega}) \end{bmatrix} d\omega \geq 0 \qquad (1)$$

where $P(e^{j\omega})$ and $Q(e^{j\omega})$ are the Fourier transform of the signals p and q respectively and $\Omega := [-\pi/T_s, \pi/T_s)$ with T_s the sampling time. From [10, Theorem 1], the feedback connection between $H \in \mathcal{RH}_\infty$ and a bounded causal operator $\mathbb{\Delta}$ (see Fig. 1) is stable if,

1) the interconnection of H and $\tau\mathbb{\Delta}$ is well-posed for all $\tau \in [0, 1]$;
2) $\tau\mathbb{\Delta}$ satisfies the IQC defined by Π for all $\tau \in [0, 1]$;
3) The following inequality is satisfied:

$$\begin{bmatrix} H(e^{j\omega}) \\ I \end{bmatrix}^* \Pi(e^{j\omega}) \begin{bmatrix} H(e^{j\omega}) \\ I \end{bmatrix} \prec 0 \qquad \forall\omega \in \Omega \quad (2)$$

Remark 1: If the upper left corner of Π is positive semi-definite and the lower right corner is negative semi-definite, then using [10, Remark 2], $\tau\mathbb{\Delta}$ satisfies the IQC defined by Π for all $\tau \in [0, 1]$ if and only if $\mathbb{\Delta}$ satisfies the IQC.

Numerous forms of multiplier matrices $\Pi(e^{j\omega})$ for different uncertainty types have been proposed in the literature [10]. Methods to directly integrate rate bounds in IQC are proposed allowing to obtain convex frequency-domain constraints which can be used for control design [10], [14], [18]. A way to present the problem of rate-bounded time-varying parameter, is to define the bounded rate as a new time-varying real scalar parameter. For rate-bounded time-varying scalar uncertainties, i.e.

$$\mathbb{\Delta}(k) = \delta(k)I, \quad |\delta(k)| \leq \eta, \quad |\delta(k) - \delta(k-1)| \leq \zeta \leq 2\eta,$$

where $\eta, \zeta > 0\ \forall k \in \mathbb{R}_+$, a stationary multiplier Π can be defined as [13]:

$$\Pi = \begin{pmatrix} \eta^2 D & 0 & E & 0 \\ 0 & \zeta^2 \bar{D} & 0 & \bar{E} \\ E^T & 0 & -D & 0 \\ 0 & \bar{E}^T & 0 & -\bar{D} \end{pmatrix}, \qquad (3)$$

where $D = D^T \succeq 0, \bar{D} = \bar{D}^T \succeq 0, E = -E^T, \bar{E} = -\bar{E}^T$.

For a given system $H(e^{j\omega})$,2 can be used to compute Π satisfying the constraint. From (3), the numerical values of η and ζ can be identified allowing to compute the bounds on the uncertainty block $\mathbb{\Delta}(k)$. Similarly, the obtained IQC can be used as a control design constraint to guarantee robustness for desired fixed upper bounds η and ζ.

B. Control design for LFT systems

A method to design fixed-structure frequency-domain controller based on linear fractional transform (LFT) representation is presented in [19]. A convex optimisation problem using LMIs is proposed to obtain an LTI controller with a fixed-structure parametrization. Since this method will be used in this paper, a summary of the main results is presented in this section.

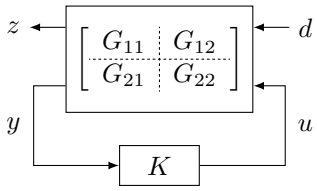

Fig. 2. LFT interconnection between generalized system and controller

The FRF of a generalized system $\mathcal{G}$ with exogenous signals $d \in \mathbb{R}^{n_d}$, control inputs $u \in \mathbb{R}^{n_u}$, measurements $y \in \mathbb{R}^{n_y}$ and performance channels $z \in \mathbb{R}^{n_z}$ can be presented as:

$$\begin{bmatrix} z \\ y \end{bmatrix} = \left[\begin{array}{c:c} G_{11} & G_{12} \\ \hdashline G_{21} & G_{22} \end{array}\right] \begin{bmatrix} d \\ u \end{bmatrix}.$$

The aim is to design an LTI controller K in order to compensate for the effect of the exogenous disturbances d on the performance channels z. The corresponding LFT represented in Fig. 2 is given by

$$T_{zd} = G_{11} + G_{12}K(I - G_{22}K)^{-1}G_{21}. \tag{4}$$

Assuming the closed-loop system is stable, the infinity norm of T_{zd} can be expressed as

$$||T_{zd}||_\infty^2 = \sup_{\omega \in \Omega} \bar{\sigma}(T_{zd}^*(e^{j\omega})T_{zd}(e^{j\omega}))$$

where $\bar{\sigma}$ is the maximum singular value. This can be evaluated if $G(e^{j\omega})$, the FRF of $\mathcal{G}$, $\forall \omega \in \Omega$ is available. As an example, an $\mathcal{H}_\infty$ control design problem can be formulated as the minimization of the spectral norm:

$$\begin{aligned} &\min_{K,\gamma} \gamma \\ &\text{s.t.} \quad T_{zd}^*(e^{j\omega})T_{zd}(e^{j\omega}) \preceq \gamma I, \qquad \forall \omega \in \Omega \end{aligned} \tag{5}$$

The controller K can be parameterized as $K = Y^{-1}X$, where X and Y are both $\mathcal{RH}_\infty$ matrix functions linear in optimization variables. Assuming that G_{12} is full column rank $\forall \omega \in \Omega$, the constraint on the spectral norm given by $T_{zd}^* T_{zd} \preceq \gamma I$ can be equivalently expressed as an LMI:

$$\begin{bmatrix} \gamma I - \Lambda & (\Phi G_{11} + XG_{21})^* \\ (\Phi G_{11} + XG_{21}) & \Phi\Phi^* \end{bmatrix} \succ \mathbf{0}, \tag{6}$$

where $\Phi = (Y - XG_{22})\, G_{12}^{\mathsf{L}}, \Lambda = (\Psi G_{11})^*(\Psi G_{11})$ and $\Psi = I - G_{12}G_{12}^{\mathsf{L}}$. This constraint is not convex and does not guarantee the closed-loop stability. It is shown in [19] that a convex lower-bound on the quadratic term $\Phi\Phi^*$ can be obtained that ensure the closed-loop stability as well:

$$\Phi\Phi^* \succeq \Phi\Phi_c^* + \Phi_c\Phi^* - \Phi_c\Phi_c^* \tag{7}$$

where $\Phi_c = (Y_c - X_cG_{22})\, G_{12}^{\mathsf{L}}$, and $K_c = Y_c^{-1}X_c$ is an initial stabilizing controller. In practice, $K_c = 0$ can be chosen for open-loop stable plants. The optimisation problem (5) can now be formulated as:

$$\begin{aligned} &\min_{X,Y,\gamma} \gamma \\ &\begin{bmatrix} \gamma I - \Lambda & (\Phi G_{11} + XG_{21})^* \\ \star & \Phi\Phi_c^* + \Phi_c\Phi^* - \Phi_c\Phi_c^* \end{bmatrix}(e^{j\omega}) \succ \mathbf{0} \quad \forall \omega \in \Omega, \end{aligned} \tag{8}$$

To solve the optimisation problem, a grid-based approach can be employed for the frequency set Ω to obtain a finite number of constraints. The results can be improved using an iterative approach where the controller K is used as the initial stabilising control for the next iteration. This sequence of convex optimisation problems converges to a local optimal solution of the original nonlinear problem. For a more detailed explanation of the method, refer to [19].

III. Main Results

A. Basic problem statement

The control system architecture is schematically presented in Fig. 4. The system to be controlled is a multivariable linear time-invariant (LTI-MIMO) plant P_2 with n_u input channels and n_y output channels. The FRF matrix can be acquired from classical system identification experiments [20]. Given n_u sets of finite sampled input/output data which can be acquired from n_u open-loop identification experiments, the corresponding discrete-time FRF can be estimated as:

$$P_2(e^{j\omega}) = \left[\sum_{k=0}^{M-1} \mathbb{Y}(k)e^{-j\omega T_s k}\right] \left[\sum_{k=0}^{M-1} \mathbb{U}(k)e^{-j\omega T_s k}\right]^{-1} \tag{9}$$

where M is the number of data points and each column of $\mathbb{U}(k)$ and $\mathbb{Y}(k)$ represents respectively the inputs and outputs at the time sample k at one experiment. It is assumed that $P_2(e^{j\omega})$ is bounded for all frequencies $\omega \in \Omega$. The estimation errors can be considered as model uncertainty and taken into account for the controller design, however, they are neglected to focus on the main subject of this paper. In addition, a stationary perturbation model $P_1(e^{j\omega})$ is used to model the propagation of an exogenous perturbation signal d to the measurement y. The disturbance signal d is assumed to be a sinusoidal signal having an unknown time-varying harmonic frequency $\rho(k)$ with a bounded rate. The objective is to design a stabilizing controller that reject asymptotically the effect of the disturbance at the output.

B. Controller structure for harmonic disturbance rejection

As the harmonic frequency of the disturbance signal is non-stationary, P_2 shall be controlled by an LPV controller with the harmonic frequency as scheduling parameter. The LPV controller is chosen as the multiplication of an LTI controller $K(z)$ and a time-varying filter $N(z, \theta(k))$:

$$K_N(z, \theta(k)) = K(z)N(z, \theta(k)),$$

where $\theta(k) \in \Theta$ is the scheduling parameter. The time-invariant part of the controller is parameterised by $K(z) = Y(z)^{-1}X(z)$ and is computed by a convex optimisation problem to guarantee closed-loop stability for all the variations in the scheduling parameter $\theta(k)$. A sliding discrete Fourier transform (SDFT) is used for the estimation of the unknown harmonic disturbance frequency (see Section IV-B). A time-varying filter $N(z, \theta(k))$ for a fixed value of $\theta(k) = \theta_c$ ensures asymptotic performance for the disturbance rejection. In accordance to the IMP, $N(z, \theta_c)$ is chosen

as an approximation of the z-transform of a sinusoidal signal:

$$N(z,\theta_c) = \frac{1}{1+\beta\theta_c z^{-1}+\beta^2 z^{-2}}, \tag{10}$$

where β is a scalar factor allowing to adjust damping of the inverted notch filter according to the desired performance. Hence, for the steady-state case with θ_c constant, robust performance is guaranteed based on the IMP. For the transitory phase, we do not consider the attenuation performance as the estimation of the scheduling parameter requires a certain time lapse for convergence. The scheduling parameter $\theta(k)$ is chosen such that $\theta(k) = -2\cos(T_s\rho(k))$ where $\rho(k)$ is the time-varying frequency of the sinusoidal disturbance. It can be defined around a fixed frequency $\bar{\theta}$ as $\theta(k) = \bar{\theta} + \delta\theta(k)$ with $|\delta\theta(k)| \leq \eta$ such that $[\theta_{\min}, \theta_{\max}] = [\bar{\theta}-\eta, \bar{\theta}+\eta]$. The variation rate $\mathring{\theta}(k) = \delta\theta(k) - \delta\theta(k-1)$ is bounded by $\mathring{\theta}(k) \leq \zeta$. In the discrete-time domain, we can relate $\theta(k)$ to its variation rate $\mathring{\theta}(k)$ as shown in Fig. 3:

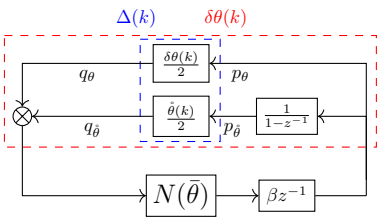

Fig. 3. Integration of $\mathring{\theta}(k)$ into $N(z,\delta\theta(k))$

This allows for an equivalent formalisation of $N(z,\theta(k)) = N(z,\theta(k),\mathring{\theta}(k))$.

For a fixed stationary value of the scheduling parameter $\theta_c = \bar{\theta} + \delta\theta_c$, $N(z,\theta_c)$ can be defined as:

$$\begin{aligned} N(z,\delta\theta_c) &= \frac{1}{1+\beta\left(\bar{\theta}+\delta\theta_c\right)z^{-1}+\beta^2 z^{-2}} \\ &= \frac{\frac{1}{1+\beta\bar{\theta}z^{-1}+\beta^2z^{-2}}}{1+\frac{\beta z^{-1}}{1+\beta\bar{\theta}z^{-1}+\beta^2z^{-2}}\delta\theta_c} \\ &= \frac{N(\bar{\theta})}{1+\beta z^{-1}N(\bar{\theta})\delta\theta_c}, \end{aligned} \tag{11}$$

As shown in (11), $N(z,\theta_c)$ can be represented as a feedback loop with $N(z,\bar{\theta})$ in the forward path and the term $\beta z^{-1}\delta\theta_c$ in the feedback. As presented in Fig. 3, $\delta\theta(k)$ and $\mathring{\theta}(k)$ can be pulled out as an uncertainty block in an LFR representation with an LTI block. Note that the LPV part of the controller is only a function of $\theta(k)$ as scheduling parameter. Therefore $\mathring{\theta}(k)$ will be used for controller synthesis and it is not required for the implementation of the algorithm.

For time-varying scheduling parameter in a multivariable system, $\delta\theta(k)$ and $\mathring{\theta}(k)$ can be replaced with $\delta\theta(k)I$ and $\mathring{\theta}(k)I$ respectively and the time-varying part of the control system can be defined by the augmented plant $\mathcal{N}$ (see Fig. 4):

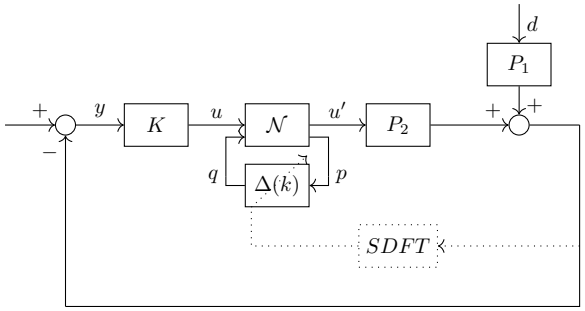

Fig. 4. Control system architecture with LTI controller part

$$\begin{aligned} \begin{pmatrix} p_\theta \\ p_{\mathring{\theta}} \\ u' \end{pmatrix} &= \begin{pmatrix} \mathcal{N}_{11} & \mathcal{N}_{12} \\ \mathcal{N}_{21} & \mathcal{N}_{22} \end{pmatrix} \begin{pmatrix} q_\theta \\ p_{\mathring{\theta}} \\ u \end{pmatrix} \\ &= \begin{pmatrix} -\frac{\beta z^{-1}}{2}N(\bar{\theta})I & -\frac{\beta z^{-1}}{2}N(\bar{\theta})I & \frac{\beta z^{-1}}{2}N(\bar{\theta})I \\ -\frac{\beta z^{-1}}{2(1-z^{-1})}N(\bar{\theta})I & -\frac{\beta z^{-1}}{2(1-z^{-1})}N(\bar{\theta})I & \frac{\beta z^{-1}}{2(1-z^{-1})}N(\bar{\theta})I \\ -N(\bar{\theta})I & -N(\bar{\theta})I & N(\bar{\theta})I \end{pmatrix} \begin{pmatrix} q_\theta \\ q_{\mathring{\theta}} \\ u \end{pmatrix}, \\ \begin{pmatrix} q_\theta \\ q_{\mathring{\theta}} \end{pmatrix} &= \Delta(k) \begin{pmatrix} p_\theta \\ p_{\mathring{\theta}} \end{pmatrix} = \begin{pmatrix} \delta\theta(k)I & 0 \\ 0 & \mathring{\theta}(k)I \end{pmatrix} \begin{pmatrix} p_\theta \\ p_{\mathring{\theta}} \end{pmatrix} \end{aligned} \tag{12}$$

C. Generalized model representation

After having "pulled out" $\delta\theta(k)$ and $\mathring{\theta}(k)$ from $\mathcal{N}$, the LTI plant model P_2 will be augmented with $\mathcal{N}$ and will be represented by an LFR. The augmented plant G^s maps $q_\theta, q_{\mathring{\theta}}$ and the control inputs u to $p_\theta, p_{\mathring{\theta}}$ and y_2 (the output of P_2) and is given by:

$$\begin{aligned} \begin{pmatrix} p_\theta \\ p_{\mathring{\theta}} \\ y_2 \end{pmatrix} &= \begin{pmatrix} G^s_{11} & G^s_{12} \\ G^s_{21} & G^s_{22} \end{pmatrix} \begin{pmatrix} q_\theta \\ q_{\mathring{\theta}} \\ u \end{pmatrix} \\ &= \begin{pmatrix} -\frac{\beta z^{-1}}{2}N(\bar{\theta})I & -\frac{\beta z^{-1}}{2}N(\bar{\theta})I & \frac{\beta z^{-1}}{2}N(\bar{\theta})I \\ -\frac{\beta z^{-1}}{2(1-z^{-1})}N(\bar{\theta})I & -\frac{\beta z^{-1}}{2(1-z^{-1})}N(\bar{\theta})I & \frac{\beta z^{-1}}{2(1-z^{-1})}N(\bar{\theta})I \\ -P_2N(\bar{\theta})I & -P_2N(\bar{\theta})I & P_2N(\bar{\theta})I \end{pmatrix} \begin{pmatrix} q_\theta \\ q_{\mathring{\theta}} \\ u \end{pmatrix} \end{aligned} \tag{13}$$

This augmented plant does not include the disturbance d and will be used to define a convex set of stabilizing controllers. The scheme representing the augmented system is given in Fig. 5.

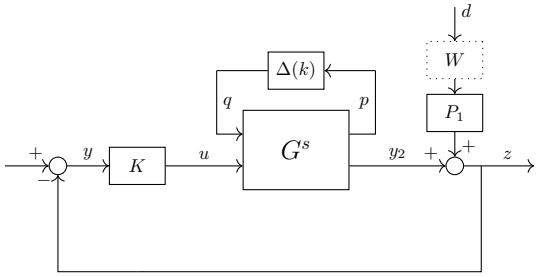

Fig. 5. Closed-loop scheme with the augmented system

Note that the time-varying filter ensures asymptotic attenuation of the disturbances. However, for nominal performance specification, high amplifications at higher frequencies should explicitly be avoided. An additional LFR for

$T_{zd}(e^{j\omega})$ can optionally be defined to constrain the effect of the external perturbation signal d on the performance channel z (see Fig. 5). The corresponding augmented plant G^p is given by

$$\begin{pmatrix} z \\ y \end{pmatrix} = \begin{pmatrix} G^p_{11} & G^p_{12} \\ G^p_{21} & G^p_{22} \end{pmatrix} \begin{pmatrix} d \\ u \end{pmatrix} \tag{14}$$

$$= \begin{pmatrix} P_1 W & P_2 N(\bar{\theta}) \\ -P_1 W & -P_2 N(\bar{\theta}) \end{pmatrix} \begin{pmatrix} d \\ u \end{pmatrix}, \tag{15}$$

where W is a weighting function which can be chosen according to the desired shape of $T_{zd}(e^{j\omega})$. In the simplest case, it can be a constant value to limit the amplification of disturbance in all frequencies.

D. Controller Design

The stability for scheduling parameter $\theta(k)$ with a rate-bounded variation $\mathring{\theta}(k)$ shall be guaranteed using an IQC-based constraint. A simplified solution for Π in accordance to (3), choosing $D = \bar{D} = I$ and $E = \bar{E} = 0$, is given by

$$\Pi_{pq} = \begin{pmatrix} \eta^2 I & 0 & 0 & 0 \\ 0 & \zeta^2 I & 0 & 0 \\ 0 & 0 & -I & 0 \\ 0 & 0 & 0 & -I \end{pmatrix}. \tag{16}$$

When inserting (16) in (2), the obtained inequality can be simplified:

$$\begin{aligned} &\begin{bmatrix} T_{pq}(e^{j\omega}) \\ I \end{bmatrix}^* \Pi \begin{bmatrix} T_{pq}(e^{j\omega}) \\ I \end{bmatrix} \prec 0 \qquad \forall \omega \in \Omega \\ \Leftrightarrow \quad &T^*_{pq}(e^{j\omega}) T_{pq}(e^{j\omega}) \prec \begin{pmatrix} \eta^{-2} I & 0 \\ 0 & \zeta^{-2} I \end{pmatrix} = U \qquad \forall \omega \in \Omega \end{aligned} \tag{17}$$

This inequality has the same form as the constraint in (5) and can be converted to a set of LMIs in the same way as for the general LFT systems presented in Section II-B and be integrated into a feasibility problem as follows:

$$\begin{aligned} &\text{Find } K \\ \text{s.t.} \quad &T^*_{zd}(e^{j\omega}) T_{zd}(e^{j\omega}) \preceq I, \quad \forall \omega \in \Omega \\ &T^*_{pq}(e^{j\omega}) T_{pq}(e^{j\omega}) \prec U \quad \forall \omega \in \Omega \end{aligned} \tag{18}$$

A feasible but undesirable solution to this problem is the controller $K = 0$. To avoid this solution, a minimal steady-state gain $g_{\min}$ of K shall be imposed. A lower-bound constraint can be formulated as follows:

$$\begin{aligned} &K(e^{j\omega})|_{\omega=0} = Y^{-1}(e^{jw})|_{\omega=0} X(e^{j\omega})|_{\omega=0} \succ g_{\min} I \\ \Rightarrow \quad &X(0) - g_{\min} Y(0) \succ 0 \end{aligned} \tag{19}$$

Based on (18) and (19), we can now define an optimisation problem maximizing η. The objective is to compute a $K(z)$ which guarantees robust stability for all $\theta(k)$ satisfying $|\delta\theta(k)| \leq \eta$ and $|\mathring{\theta}(k)| \leq \zeta$. The constraints in (18) can now be transformed into LMI in the form of (6) using the method presented in Section II-B.

The procedure to obtain the desired controller $K(z)$ is summarized in Algorithm 1. An iterative approach is proposed to reduce the conservatism related to the choice of the initial controller $K_c = 0$. At each new iteration, K_c is initialized with the optimal controller of the last iteration. $\epsilon > 0$ must be chosen sufficiently small such that the problem is feasible. Theoretically, the optimisation problems in this paper are formulated using frequency-domain constraints. They correspond to convex semi-infinite programs (SIP). A possible approach to solve such SIP is to sample the infinite number of constraints for the complete Ω at a large finite set of frequencies with a reasonable amount of frequency points $\Omega_f = \{\omega_1, \ldots, \omega_f\}$ [21].

Algorithm 1 LPV control design algorithm

Require: $K_c = 0$
Require: $\eta_1, \zeta > 0$
while $\eta_i - \eta_{i-1} > \epsilon$ **do**

- $\max\limits_{\eta_i, X, Y} \quad \eta_i$

s.t. $\begin{pmatrix} U - \Lambda & (\Phi G^s_{11} + X G^s_{21})^* \\ \star & \Phi^s (\Phi^s_c)^* + \Phi^s_c (\Phi^s)^* - \Phi^s_c (\Phi^s_c)^* \end{pmatrix} \succ 0,$

$\begin{pmatrix} I - \Lambda & (\Phi^p G^p_{11} + X G^p_{21})^* \\ \star & \Phi^p (\Phi^p_c)^* + \Phi^p_c (\Phi^p)^* - \Phi^p_c (\Phi^p_c)^* \end{pmatrix} \succ 0$

$\forall \omega \in \Omega_N,$

where $\Phi^p = (Y - X G^p_{22}) (G^p_{12})^{\mathsf{L}},$

$\Phi^s = (Y + X G^s_{22}) (G^s_{12})^{\mathsf{L}},$

$U = \begin{pmatrix} \eta_i^{-2} I & 0 \\ 0 & \zeta^{-2} I \end{pmatrix},$

$X(\omega_1) - g_{\min} Y(\omega_1) \succ 0,$

- $K_c = Y^{-1} X$
- Increment i

end while

The choice of Π as presented in (16) is conservative because the off-diagonal terms are set to zero. Hence, the achievable η is somewhat larger then the value obtained with Algorithm 1. The conservatism can be reduced using a full parameterized Π given by (3). Algorithm 2 can be used after the completion of Algorithm 1 to obtain a stability guarantee for an interval bound $\eta_{\max}$ which is larger than η_n obtained from the Algorithm 1 after n iterations. Algorithm 2 can be solved using a bisection approach or by iteratively increasing the value of η and checking the problem's feasibility.

IV. Experimental Results

A. Hybrid micro-vibration damping platform (MIVIDA)

Novel high-precision optical instruments designed for Earth observation missions require exceptional pointing accuracy. These stringent line-of-sight stability demands impose constraints on the allowable levels of mechanical vibration that may occur onboard spacecraft. Micro-vibrations, stemming from primary satellite systems such as reaction wheels, thrusters, cryocoolers, or solar array drive mechanisms can significantly degrade the performance of sensitive payloads.

Algorithm 2 Stability analysis of final controller

$$\max_{\Pi,\eta_{\max}} \quad \eta_{\max}$$

$$\text{s.t.} \begin{bmatrix} T_{pq}(e^{j\omega}) \\ I \end{bmatrix}^* \Pi \begin{bmatrix} T_{pq}^*(e^{j\omega}) \\ I \end{bmatrix} \prec 0 \qquad \forall \omega \in \Omega_N,$$

$$\begin{bmatrix} I \\ \eta_{\max} I \end{bmatrix}^* \Pi \begin{bmatrix} I \\ \eta_{\max} I \end{bmatrix} \succ 0, \qquad \forall \omega \in \Omega_N,$$

$$\Pi = \begin{pmatrix} \eta_{\max}^2 D & 0 & E & 0 \\ 0 & \zeta^2 \bar{D} & 0 & \bar{E} \\ E^* & 0 & -D & 0 \\ 0 & \bar{E}^T & 0 & -\bar{D} \end{pmatrix},$$

$$\text{where } D = D^T \succeq 0,\ \bar{D} = \bar{D}^T \succeq 0,$$

$$E = -E^T,\ \bar{E} = -\bar{E}^T$$

To address this problem, a hybrid active-passive micro-vibration damping platform (MIVIDA) was developed at CSEM. The platform aims to mitigate micro-vibrations and isolate sensitive optical payloads from external disturbances, facilitating the study of stabilizing sensitive active payloads against multiple unknown external perturbations in a broader context. The modular platform comprises an adjustable number of passive dampers, a set of proof mass actuators (PMA) generating a 6 degree of freedom (DoF) force tensor, and a payload interface capable of accommodating various types of sensitive instruments. Utilizing accelerometer measurements in close proximity to the payload, the platform actively rejects disturbances originating from the satellite body. These external perturbations are induced using an external inertial shaker. An illustration of the system is provided in Fig. 6.

All experimental evaluations of the platform are conducted at the Microvibration Characterisation Facility at CSEM in Neuchâtel, Switzerland [22].

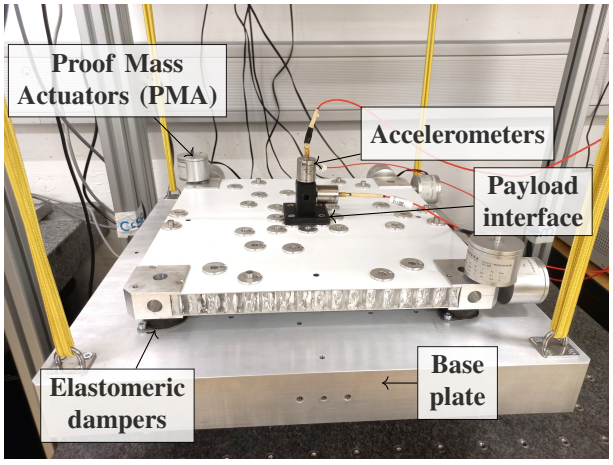

Fig. 6. Hybrid micro-vibration damping platform MIVIDA developed at CSEM, Switzerland

B. Scheduling parameter estimation

The scheduling parameter is updated by estimating the main harmonic frequency of the perturbation. As the perturbation signal d cannot be measured directly, an estimation of the harmonic frequency is calculated based on a sliding discrete Fourier transform (SDFT) on the output signal y. The SDFT is implemented using the algorithm presented in [23]. The discrete Fourier transform (DFT) is given by

$$\mathcal{Y}_n = \sum_{k=0}^{N-1} y(k) e^{-(\frac{j2\pi kn}{N})},$$

where $0 \leq n \leq N-1$ designating the n^{th} bin of the N-point DFT. The DFT can be computed recursively using the SDFT algorithm. Essentially, the SDFT algorithm arises from the fact that for two successive times $k-1$ and k, the sequences $y(k-1)$ and $y(k)$ contain mainly identical elements. The recursive update step of the SDFT at time k can therefore be expressed by

$$\mathcal{Y}_n(k) = e^{\frac{j2\pi n}{N}} \big(\mathcal{Y}_n(k-1) + y(k) - y(k-N)\big).$$

The detailed derivation of the SDFT algorithm is given in [17]. Based on the m highest peaks present in $\hat{Y}(k)$, n harmonic frequencies $\rho_i, i = 1, ..., m$ are identified in real-time. The values of ρ_i are then used to update the value of $\theta_i(k) = -2\cos T_s \rho_i(k)$.

C. Harmonic disturbance rejection on MIVIDA

To validate the method, a controller for the MIVIDA platform allowing to adaptively reject sinusoidal disturbances is computed. A system identification experiment is conducted to compute an FRF matrix $P_2(e^{j\omega})$ from experimental data using a frequency grid with 500 points and a sampling frequency of 1 kHz. The disturbance signal d is known to contain a single main harmonic frequency. Hence, a single scheduling parameter $\theta(k)$ is identified and used in $N(z, \theta(k))$. For the control design, a controller order of 40, a minimal steady-state controller gain $g_{\min} = 1$, a center frequency $\bar{\rho}$ of 60 Hz and η_0 of 0.1 Hz is used. The upper bound on the rate is set at $\zeta = 1$ Hz and the damping parameter β for $N(z, \theta(k))$ at $\beta = 0.997$. This is the highest value of β leading to a feasible solution for this application. The performance weighting factor W is chosen as $W = -10I$ dB in order to limit the infinity norm of the sensitivity function

$$S(e^{j\omega}, \bar{\theta}) = [I + P_2(e^{j\omega}) K_N(e^{j\omega}, \bar{\theta})]^{-1}.$$

The identified FRF matrices $P_1(e^{j\omega})$ and $P_2(e^{j\omega})$ together with the computed sensitivity function $S(e^{j\omega}, \theta)$ are presented in Fig. 7. It can be observed that the disturbance frequency is attenuated mostly at around 25 dB along the three axes. The obtained controller guarantees stability for a value of $\rho(k) \in [16, 104]$ Hz. This is the resulting value obtained with Algorithm 2, the stability interval obtained after the last iteration with Algorithm 1 is $\rho(k) \in [54, 66]$ Hz. To assess this result of guaranteed stability for $\rho(k) \in [16, 104]$ Hz, it can be compared to the stability interval of

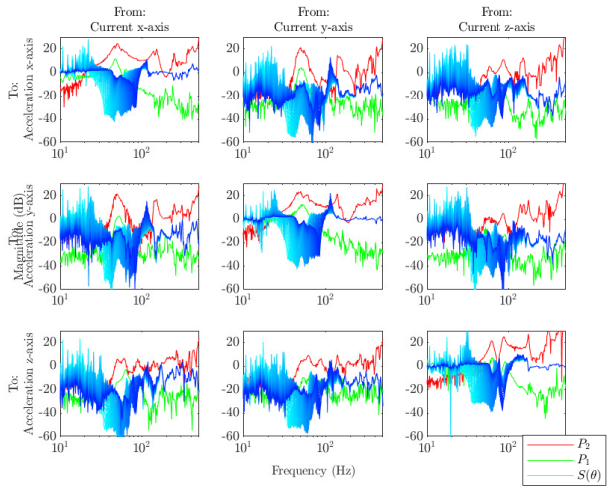

Fig. 7. Closed-loop sensitivity functions $S(\theta)$ and FRF matrix of perturbation model P_1 and of plant model P_2

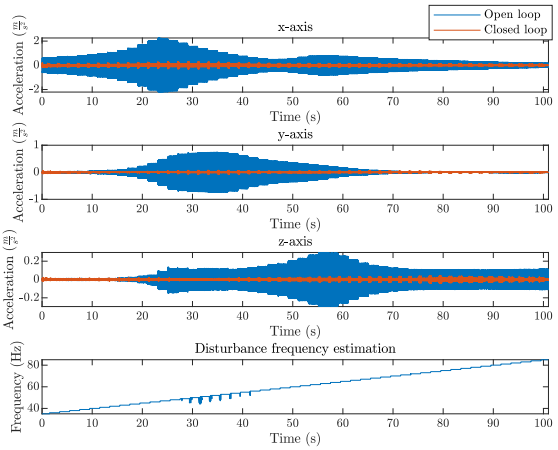

Fig. 8. Closed-loop attenuation test

$\rho(k) \in [44, 76]$ Hz that was achieved for an arbitrarily fast scheduling parameter variation on the same setup (results presented in [17]). Hence, a significant increase in the disturbance frequency interval $\rho_{\max}$ can be achieved by introducing rate bounds on the scheduling parameter $\theta(k)$.

The closed-loop control system including the real-time scheduling-parameter estimation and sensor data acquisition is implemented using a dSpace rapid prototyping platform. Two individual power amplifiers generate the power supply and the analog input and output signals for the PMA and the accelerometers respectively. A third control module is used for the command of the external inertial shaker. For performance evaluation, a sinusoidal perturbation along the x-axis is injected with this shaker. In Fig. 8, the measured accelerations along the three axes in open- and closed-loop are shown. The harmonic frequency $\rho(k)$ of the sinusoidal perturbation is shifted in the interval of $\rho(k) \in [35, 85]$ Hz increasing the frequency by 1 Hz every 2 seconds. The frequency range of the sinusoidal perturbation could be theoretically further extended according to the achieved stability interval for $\rho(k) \in [16, 104]$. However, due to physical limitations such as limited sensitivity of the accelerometer and the nonlinear behaviour of the PMA close to their resonance frequency at around 25 Hz, the zones closer to the limit of the interval cannot be implemented. Table 1 shows the obtained attenuation values for different values of $\rho(k)$.

An additional test has been performed to assess the closed-loop stability for a faster variation of the scheduling parameters $\theta(k)$ which is above the rate bound ζ. During that test, the harmonic frequency $\rho(k)$ of the sinusoidal perturbation is increased by 10 Hz every 5 seconds in the interval of $\rho(k) \in [35, 85]$. From Fig. 9, it can be observed that the stability is still guaranteed in closed-loop. Note that the attenuation performance cannot be always achieved and the transitory phase is somewhat longer. However, the stability of the closed-loop is still guaranteed even if there may be slight amplifications compared to the open loop response.

	Attenuation Performance (dB)		
	X-axis	Y-axis	Z-axis
$\rho(k) = \bar{\rho} = 60$ Hz	17.42	25.23	25.57
$\rho(k) = 35$ Hz	15.56	-2.50	-4.81
$\rho(k) = 40$ Hz	21.06	10.34	1.13
$\rho(k) = 50$ Hz	22.47	32.80	27.01
$\rho(k) = 70$ Hz	21.09	8.62	22.12
$\rho(k) = 80$ Hz	17.71	9.51	18.89
$\rho(k) = 85$ Hz	14.28	2.99	23.21

TABLE I

ATTENUATION PERFORMANCE ACHIEVED WITH THE IQC-BASED LPV CONTROLLER AT DIFFERENT VALUES OF $\rho(k)$

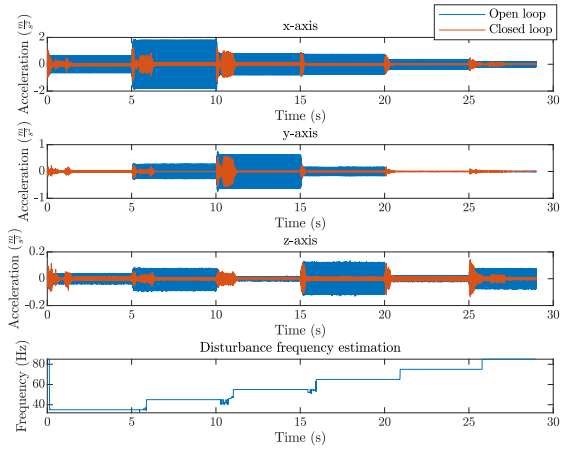

Fig. 9. Fast parameter variation test

V. Conclusions

A data-driven method to compute an LPV controller with rate-bounded scheduling parameter variation was developed and validated on a hardware system. Using an IQC describing a time-varying real scalar with rate bound, an equivalent LMI is computed which is included in a two-step iterative control design algorithm. This method allows to guarantee the stability of the controller for time-varying scheduling parameters lying in a bounded interval and varying at a bounded rate. Based on an FRF matrix of an LTI-MIMO system, an LPV controller is computed for adaptive rejection of a non-stationary sinusoidal disturbance signal with an unknown harmonic frequency. A controller was designed for the hybrid micro-vibration damping (MIVIDA) platform using the proposed method. The closed-loop stability is guaranteed up to a scheduling parameter variation rate of 1 Hz. The resulting controller achieves a disturbance attenuation of up to 32.80 dB on the real system and the closed-loop stability is experimentally verified.

References

[1] H. E. Tseng and D. Hrovat, "State of the art survey: active and semi-active suspension control," *Vehicle System Dynamics*, vol. 53, no. 7, pp. 1034–1062, 2015. [Online]. Available: http://www.tandfonline.com/doi/full/10.1080/00423114.2015.1037313

[2] Q. Zheng, L. Dong, D. H. Lee, and Z. Gao, "Active disturbance rejection control for MEMS gyroscopes," *IEEE Transactions on Control Systems Technology*, 2009.

[3] R. Fareh, S. Khadraoui, M. Y. Abdallah, M. Baziyad, and M. Bettayeb, "Active disturbance rejection control for robotic systems: A review," *Mechatronics*, vol. 80, p. 102671, 2021. [Online]. Available: https://linkinghub.elsevier.com/retrieve/pii/S0957415821001392

[4] V. Nguyen, J. Johnson, and S. Melkote, "Active vibration suppression in robotic milling using optimal control," *International Journal of Machine Tools and Manufacture*, vol. 152, 2020. [Online]. Available: https://linkinghub.elsevier.com/retrieve/pii/S0890695519312623

[5] T.-B. Airimitoaie, I. D. Landau, R. Melendez, and L. Dugard, "Algorithms for adaptive feedforward noise attenuation—a unified approach and experimental evaluation," *IEEE Transactions on Control Systems Technology*, vol. 29, no. 5, pp. 1850–1862, 2021. [Online]. Available: https://ieeexplore.ieee.org/document/9203846/

[6] P. Ballesteros and C. Bohn, "Disturbance rejection through LPV gain-scheduling control with application to active noise cancellation," *IFAC Proceedings Volumes*, vol. 44, no. 1, pp. 7897–7902. [Online]. Available: https://linkinghub.elsevier.com/retrieve/pii/S1474667016448779

[7] S. S. Madani and A. Karimi, "Data-driven LPV controller design for islanded microgrids," *IFAC-PapersOnLine*, vol. 54, no. 7, pp. 433–438, 2021. [Online]. Available: https://linkinghub.elsevier.com/retrieve/pii/S2405896321011721

[8] T. Bloemers, T. Oomen, and R. Tóth, "Frequency Response Data-Driven LPV Controller Synthesis for MIMO Systems," *IEEE Control Systems Letters*, vol. 6, pp. 2264–2269, 2022.

[9] P. Schuchert and A. Karimi, "Frequency-domain data-driven position-dependent controller synthesis for cartesian robots," *IEEE Transactions on Control Systems Technology*, vol. 31, no. 4, pp. 1855–1866, 2023. [Online]. Available: https://ieeexplore.ieee.org/document/10081199/

[10] A. Megretski and A. Rantzer, "System analysis via integral quadratic constraints," *IEEE Transactions on Automatic Control*, vol. 42, no. 6, pp. 819–830, Jun. 1997.

[11] T. Bloemers, T. Oomen, and R. Toth, "Frequency response data-based lpv controller synthesis applied to a control moment gyroscope," *IEEE Transactions on Control Systems Technology*, vol. 30, no. 6, pp. 2734–2742, Nov. 2022.

[12] U. Jonsson and A. Rantzer, "Systems with uncertain parameters-time-variations with bounded derivatives," in *Proceedings of 1994 33rd IEEE Conference on Decision and Control*, vol. 3. Lake Buena Vista, FL, USA: IEEE, 1994, pp. 3074–3079. [Online]. Available: http://ieeexplore.ieee.org/document/411313/

[13] J. M. Fry, D. Abou Jaoude, and M. Farhood, "Robustness analysis of uncertain time-varying systems using integral quadratic constraints with time-varying multipliers," vol. 31, no. 3, pp. 733–758. [Online]. Available: https://onlinelibrary.wiley.com/doi/10.1002/rnc.5299

[14] U. Jönsson, "Robustness Analysis of Uncertain and Nonlinear Systems," Doctoral Thesis (monograph), Department of Automatic Control, Lund Institute of Technology (LTH), 1996.

[15] A. Helmersson, "An IQC-based stability criterion for systems with slowly varying parameters," *IFAC Proceedings Volumes*, vol. 32, no. 2, pp. 3183–3188, Jul. 1999. [Online]. Available: https://linkinghub.elsevier.com/retrieve/pii/S147466701756543X

[16] J. Veenman, C. W. Scherer, and H. Köroğlu, "Robust stability and performance analysis based on integral quadratic constraints," *European Journal of Control*, vol. 31, pp. 1–32, Sep. 2016. [Online]. Available: https://linkinghub.elsevier.com/retrieve/pii/S0947358016300097

[17] E. Klauser and A. Karimi, "Data-driven LPV Control for Micro-disturbance Rejection in a Hybrid Isolation Platform," *IEEE Transactions on Control Systems Technology*, 2024 (under review).

[18] A. Megretski, "Frequency-domain criteria of robust stability for slowly time-varying systems," *IEEE Transactions on Automatic Control*, vol. 40, no. 1, pp. 153–155, Jan. 1995. [Online]. Available: http://ieeexplore.ieee.org/document/362880/

[19] P. Schuchert, V. Gupta, and A. Karimi, "Data-driven fixed-structure frequency-based $\mathcal{H}_2$ and $\mathcal{H}_\infty$ controller design," 2023 (manuscript submitted for publication). [Online]. Available: https://infoscience.epfl.ch/record/301390

[20] R. Pintelon and J. Schoukens, *System Identification: A Frequency Domain Approach*, 2nd ed. John Wiley & Sons, Ltd, 2012.

[21] P. Schuchert and A. Karimi, "Robust Data-Driven Controller Design with Finite Frequency Samples," 2024 (under review).

[22] E. Onillon, T. Adam, G. B. Gallego, and E. Klauser, "CSEM micro-vibration characterisation facility description and validation," in *European Space Mechanisms and Tribology Symposium (ESMATS)*, Warsaw, Poland, Sep. 2021.

[23] R. Lyons, "dsp tips & tricks - the sliding DFT," *IEEE Signal Processing Magazine*, vol. 20, no. 2, pp. 74–80, 2003. [Online]. Available: http://ieeexplore.ieee.org/document/1184347/